# Experimental Investigation of the Triple-Junction Effect on the Electric Discharge Characteristics and Modeling of the Maximum Discharge Current

**Nabila Saim**† and **Ferroudja Bitam-Megherbi**, Non-members


## ABSTRACT

The electrical discharge and breakdown characteristics of a triple junction (TJ) in high voltage (HV) electrical insulation are becoming an important issue in recent industrial applications. In this paper, a comparative study is conducted between three insulation materials used in HV: silicone, porcelain, and heat tempered glass, with electrode shape parameters such as inter-electrode distance ($d$), applied voltage ($V$), and geometry investigated for positive polarity, using an experimental approach. For optimum test organization to support our research and highlight the parameters and their interactions, we have established a mathematical regression model of the discharge current. It is polynomial, with good performance and a high level of precision. Besides, this yields one monovariable and another two-variable quadratic model. The latter can simulate the electric discharge simultaneously with two variables: $V$ and $d$, and an adjusted determination coefficient ($R^2_{adj}$) of nearly 0.99. Consequently, the two-variable quadratic model has been adapted to $V$ and $d$ ranges of 10 to 50 kV and 1.9 to 8 cm, respectively. Finally, this study provides us with new applicable knowledge about the TJ effect on electrical insulation with recommendations to optimize the design for higher performance.


**Keywords**: Electrical Discharge Current, Electric Field, Model, Solid Insulator, Triple Junction

## 1. INTRODUCTION

The triple point, also called a triple junction (TJ), is formed where three different materials are present, mainly at a gas/solid insulator/electrode junction. The TJ is considered to be the cause of insulation breakdown [1, 2] since it is often the weakest point of the insulator. Indeed, the electric field is enhanced by the insulation. This is mainly due to the mismatch between the permittivity of the metal, solid insulator, and gas. If these regions are not carefully designed, partial discharge (PD) may appear, accelerating the aging process of the insulator [3]. Furthermore, the study of PDs in TJ geometry is important for good control of system reliability [4–6].

Triple points are present in numerous HV and medium voltage applications. During their exploitation, TJs are exposed to different constraints such as mechanical, environmental, chemical, thermal, and electrical. Consequently, knowledge of the mechanisms involved in the generation and propagation of electrical discharge at the TJ is an important step for achieving good optimization of this equipment. By increasing the electric field at the triple point, the first ionization process occurs and the emitted electrons hit the solid insulator, causing load accumulation on the insulating surface [7, 8]. The flashover process is assumed to be triggered on the insulator surface by secondary electron emission valanche (SEEA) mechanisms. The source of the SEEA is also assumed to be the field emitted electron from the highly stressed triple point [9]. Therefore, different designs have been developed using shapes and material modifications to eliminate the field emission electrons from TJs [10–13]. Beroual *et al.* [14], Handala *et al.* [15], and Abahazem *et al.* [16] treated electrical discharge using different point-plane electrode systems with various insulators, opening the way for practical and theoretical reflection by researchers in this field. A theoretical model has been proposed to explore the curvature effects of small radius regions on breakdown characteristics, thus providing an accurate and reasonable estimation of the optimized design parameters. The proposed model achieves a good trade-off between simplicity and accuracy [17]. However, such results need further experimental validation. The TJ has a critical influence on withstanding the voltage level of the insulating gap [1–18]. An investigation has been conducted concerning the effect of TJ on discharge characteristics such as breakdown voltage. The

Manuscript received on July 2, 2020 ; revised on December 14, 2020 ; accepted on December 14, 2020. This paper was recommended by Associate Editor Kriangkrai Sooksood.

The authors are with the Laboratory of Electrical Engineering Advanced Technologies (LATAGE), Mouloud Mammeri University of Tizi-Ouzou, Algeria.

†Corresponding author: nabila_saim@yahoo.fr



Digital Object Identifier 10.37936/ecti-eec.2021192.241328

***Fig. 1:*** *Proposed experimental device.*


(a) (b)

***Fig. 2:*** *Sample cutting mode: (a) vertical cut and (b) horizontal cut.*

effect of the voltage waveform and the insulating materials used (glass, polycarbonate, polyethylene, polypropylene, Bakelite, and toughened glass) on the morphology and length of discharge have been studied over solid/liquid insulating surfaces in a point-plane electrode arrangement [14]. The insulating materials have been shown to significantly influence the discharge properties, especially their morphology. However, synthetic materials such as silicone have recently been adopted in industrial applications due to their proven breakdown characteristics, but their long-term performance is still not completely understood and needs further investigation. The effect of distance between the discharge axis and TJ on the discharge ignition time has been evaluated. In addition, different ceramic materials with various relative permittivity have been studied, analyzing the optimum distance between the discharge axis and the TJ [19].

This current work consists of an experimental study of electrical discharge in the TJ at atmospheric pressure against the inter-electrode distance ($d$), applied voltage ($V$), geometry of the active electrode and electrical permittivity. Indeed, we have examined the electrical problems produced by the TJ through measuring the maximum discharge current ($I_0$) and subsequently developing a regression model for electrical discharge at the TJ. This model is a characterization of the experiments carried out in our study. In addition, we compare the monovariable and two-variable quadratic model, validating and applying the latter for $V$ and $d$ ranges of 10 to 50 kV and 1.9 to 8 cm, respectively. Finally, an attempt is made to reduce the electrical discharge by improving the design of the electrical insulators. This work provides us with more reliable and applicable results on complex questions related to triple points.

## 2. EXPERIMENTAL AND MATHEMATICAL APPROACH

### 2.1 Experimental Device

To conduct experiments on different samples with precision, for the first time, we have developed the device shown in Fig. 1, allowing us to set and vary $d$, one being pointed: HV end and the other planar: ground end. The HV end is made from Z200 of hard steel measuring 19 cm in length, 6 mm in diameter ($D_p$), with a straight part of 12 cm, while the other 7 cm part is inclined at an angle of 135°. It ends with a curvature tip radius ($r$) of 0.15 mm and a solid angle of 21.4°. We have realized 7 points of $r$ (see Section 3.1.3) by varying the length of the pointed part using a machine called a profile projector. The ground end is also made from Z200 of hard steel, rectangular in shape measuring 10.4 cm in length, 0.7 cm in width, and 0.16 cm in height to channel the field in one direction. The specimen position is also variable. The support for this electrode system is based on polymethyl methacrylate and Bakelite.

### 2.2 Materials Used as Solid Insulators and Sample Cutting Mode

Our silicone, porcelain, and heat tempered glass samples come from the insulators used in HV. The mode of cutting is illustrated in Fig. 2.

### 2.3 Experimental Setup

The experimental setup used in this study is shown in Fig. 3. The HV is provided by a single-phase test transformer with the following characteristics: $U = 100$ kV, $f = 50$ Hz, $S = 10$ kVA. The HV end is connected to the HV terminal of the transformer with

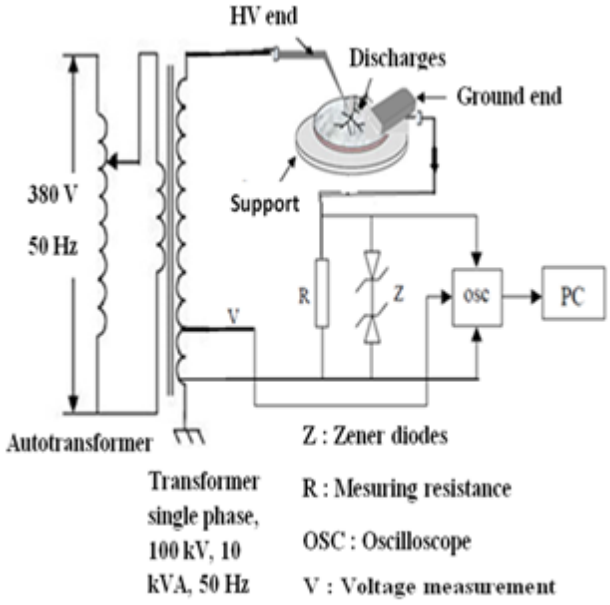


***Fig. 3:*** *Experimental setup.*

the end grounded. To avoid side effects, the edges of the ground end are rounded. The transformer and the test cell are placed in a Faraday cage. The voltage is varied with a potentiometer, located in the control panel. The discharge current is obtained from the voltage across a resistance of 48.6 kW. This voltage is obtained by means of a digital storage oscilloscope with an input impedance of 1 MΩ and different sample used for each test, performed under the following average conditions: atmospheric pressure 1010 hPa, relative humidity level 63.4%, and temperature 15 °C.

### 2.4 Mathematical Model

This section details the mathematical approach used to develop an electrical discharge model at the TJ. This model is a characterization of the experiments carried out in our study [20, 21].

#### 2.4.1 General model of maximum discharge current

According to the experimental results illustrated in Figs. 4, 5, and 6, two types of relations of $I_0$ are distinguished namely, linear dependence concerning $r$ and non-linear dependence concerning $V$ and $d$. Since this non-linearity is different, we opted for the general model of $I_0$ given by Eq. (1) ($I_0$ in $\mu$A). Regression analysis was performed to obtain our model. It is therefore a polynomial that can be assigned for both linear and non-linear relations (as a function of $N$), valid for the three materials: silicone, porcelain, and heat tempered glass, according to the variable under study and the degree of its non-linearity. In addition, it is simple and results in an optimization problem that is easy to solve [22, 23].

$$f(x) = \sum_{i=0}^{N} a_i x^i \tag{1}$$

where $x$ are the independent variables: $r$ (mm), $d$ (cm), and $V$ (kV); $a_i$ and $N$ are the coefficients and degrees of the model to be determined.

After specifying the model, we will identify $N$ and $a_i$ for each variable $r$, $d$, and $V$.

#### 2.4.2 Identification of $N$ and $a_i$

We will identify $N$ as a type of dependence function (linear/non-linear) and the severity of this non-linearity [24]. For $N = 1$, we have a linear model.

In order to find the coefficients $a_i$ of our model, a simple optimization problem needs to be solved [25]. In this section, we provide details of this procedure. For samples $y_i$ ($i = 1, \ldots, M$: $M$ is an integer) of a function to be modeled, depending on the variable $x$ which itself has samples $x_i$ ($i = 1, \ldots, M$), Eq. (2) can be written as:

$$\begin{aligned} y_1 &= \textstyle\sum_{i=0}^{N} a_i x_1^i \\ y_2 &= \textstyle\sum_{i=0}^{N} a_i x_2^i \\ &\vdots \\ y_M &= \textstyle\sum_{i=0}^{N} a_i x_M^i \end{aligned} \tag{2}$$

This system of equations can be put into matrix form, as follows:

$$\begin{bmatrix} y_1 \\ y_2 \\ \vdots \\ y_M \end{bmatrix} = \begin{bmatrix} 1 & x_1 & \cdots & x_1^N \\ 1 & x_2 & \cdots & x_2^N \\ \vdots & \vdots & \ddots & \vdots \\ 1 & x_M & \cdots & x_M^N \end{bmatrix} \begin{bmatrix} a_0 \\ a_1 \\ \vdots \\ a_N \end{bmatrix} \tag{3}$$
$$\mathbf{y} = \mathbf{X}\mathbf{a}$$

To obtain the coefficients $a_i$ or simply the vector $\mathbf{a}$ minimizing the sum of the squared errors (between observations and models), the following optimization problem must be solved:

$$\text{minimize } ||y - Xa||_2^2 \tag{4}$$

where $||.||$ is the $\ell_2$ norm of a vector.

This problem is solvable by taking the pseudo-inverse of the matrix $\mathbf{X}$. Consequently, the optimal solution $\mathbf{a}$ is given by Eq. (5):

$$\mathbf{a} = \left(\mathbf{X^T X}\right)^{-1} \mathbf{X^T y} \tag{5}$$

#### 2.4.3 Monovariable model of the maximum discharge current independently associated with $V$, $d$, and $r$

The model of $I_0$ for each independent variable $V$, $d$, and $r$ and the three selected materials is taken and calculated from the general model

(Eq. (1)) and presented in Eq. (6) to characterize the experiments carried out as shown in Figs. 4, 5, and 6, respectively. For $x = d$: $N = 4$, $d = (3.9, 3.6, 3.4, 2.9, 2.6, 2.4, 2.2, 1.9)$ cm, $V = 12$ kV, and $r = 0.15$ mm. For each selected $d$ (3.9, 3.4, 2.9, 2.4, 1.9 cm) and $x = V$: $N = 7$, $V = (4, 4.5, 5, 5.5, 6, 6.5, 7, 7.5, 8, 8.5, 9, 9.5, 10, 12)$ kV, and $r = 0.15$ mm. Finally for $x = r$: $N = 1$, $r = (0.15, 0.18, 0.2, 0.4, 0.6, 0.8, 1)$ mm, $d = 2.9$ cm, and $V = 12$ kV.

$$I_0 = \sum_{i=0}^{N} a_i x^i \tag{6}$$

#### 2.4.4 Quadratic model with variables $V$ and $d$ of the maximum discharge current

The quadratic model of $I_0$ corresponds to the variables $V$ and $d$ obtained for $r = 0.15$ mm, $V = (4, 6, 8, 10, 12)$ kV, $d = (3.9, 3.4, 2.9, 2.4, 1.9)$ cm, and each selected material, characterizing the experiments conducted in Figs. 4 and 5, and calculated on the basis of the general model (Eq. (1)). This model is represented by Eq. (7). The fluctuation in variable $r$ is not considered due to the complexity of the experimental realization.

$$I_0 = a_0 + a_1(d^2) + a_2(V \times d) + a_3(d) + a_4(V) \tag{7}$$

## 3. RESULTS AND DISCUSSION

### 3.1 Results of the Experimental Approach

#### 3.1.1 Influence of the inter-electrode distance on the maximum discharge current

In order to evaluate its effect on $I_0$, $d$ is varied between 1.9 and 3.9 cm, with the measurement performed under $V = 12$ kV. Then, $I_0$ is measured for the three samples of silicone, porcelain, and heat tempered glass; the results of which are shown in Fig. 4.

In Fig. 4, it can be observed that $I_0$ decreases as $d$ increases for the three samples. Similar variations have been observed by Larsson *et al.* [26].

Fig. 4 shows that the amplitude of the positive impulses falls rapidly with $d = 1.9$ cm rising to 2.9 cm. With this increase in $d$ value, the discharge current decrease is much lower. However, this result depends strongly on the value of the electric field at the TJ [19].

Indeed, for intense electric field zones (smaller $d$), the discharge regime is important due to high electronic activation, which boosts the streamer propagation, thus involving a larger $I_0$. Moreover, for a weak electric field zone (increase of $d$), the space between electrode dielectrics undergoes a fall in discharge activity due to a small probability of apparition in the ionization process. In other words, electronic attachment is predominant, and therefore the value of $I_0$ is smaller [27].

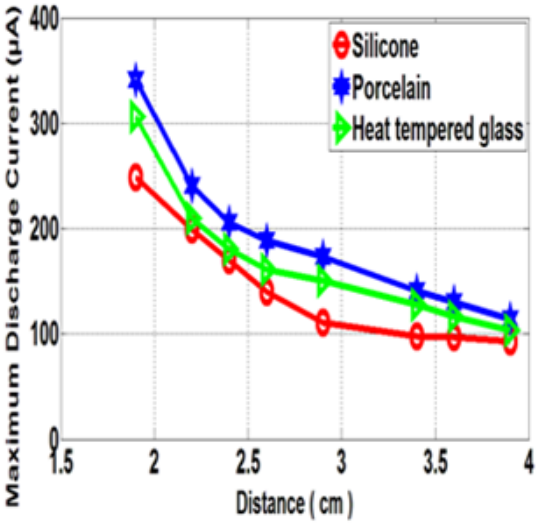


***Fig. 4:*** *Variation of $I_0$ against d: HV end in Z200 steel, with $D_p = 6$ mm, $r = 0.15$ mm, and $V = 12$ kV.*

In addition, the amplitude of positive porcelain impulses was observed to be higher than that of heat tempered glass and silicone. This can be explained by positive streamers developing over a greater distance than those of heat tempered glass and silicone [28].

#### 3.1.2 Influence of the applied voltage on the maximum discharge current

The voltage has been varied between 4 and 10 kV, with the measurement performed for $d$ between 1.9 and 3.9 cm. Subsequently, $I_0$ was measured for three samples of silicone, porcelain, and heat tempered glass; the results of which are shown in Fig. 5. As can be seen, Figs. 5(a), 5(b), 5(c), 5(d), and 5(e) show $I_0$ increases with $V$ for the selected materials.

This increase can be explained by the phenomenon of accumulated electrical charge at the TJ, due to the strengthening of the electric field at the surface under study, giving rise to discharge in this zone [15, 16, 29].

Indeed, the electric field depends linearly on $V$ to the TJ. The greater the increase in $V$, the higher the electric field. More electrons will be energetic, making the amplification of the electronic avalanche stronger and faster [30]. This leads to an increase in $I_0$. The same phenomena have also been observed in the research by Javadiz *et al.* [31], Kozlov *et al.* [32], Eichwald *et al.* [33], and Larsson *et al.* [26].

#### 3.1.3 Influence of the tip curvature radius on the maximum discharge current

In order to evaluate its effect on $I_0$, $r$ is varied between 0.15 and 1 mm, with the measurement performed under $V = 12$ kV and $d = 2.9$ cm. Then, $I_0$ is measured for the three samples of silicone, porcelain, and heat tempered glass; the results of

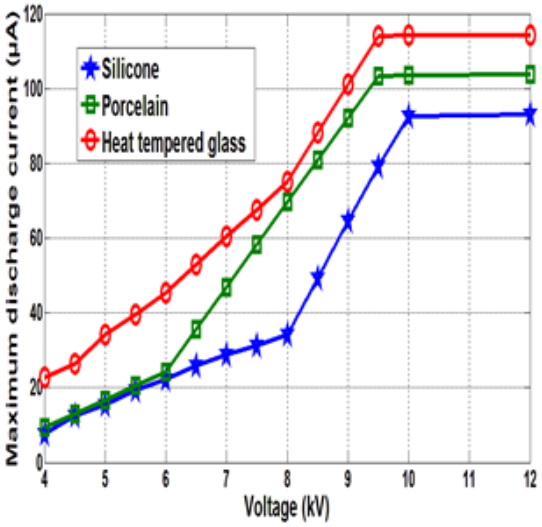


(a) $d = 3.9\,\text{cm}$

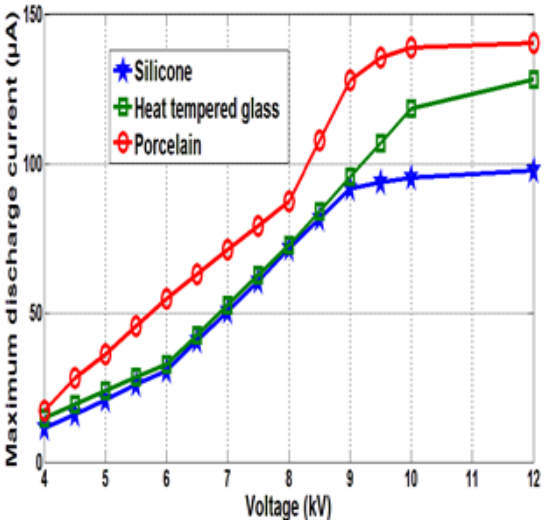


(b) $d = 3.4\,\text{cm}$

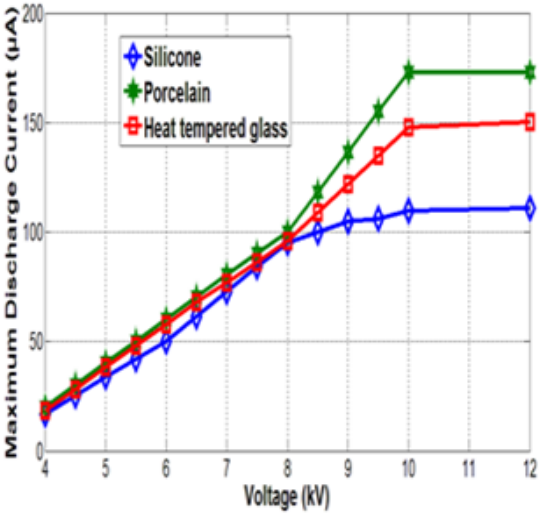


(c) $d = 2.9\,\text{cm}$

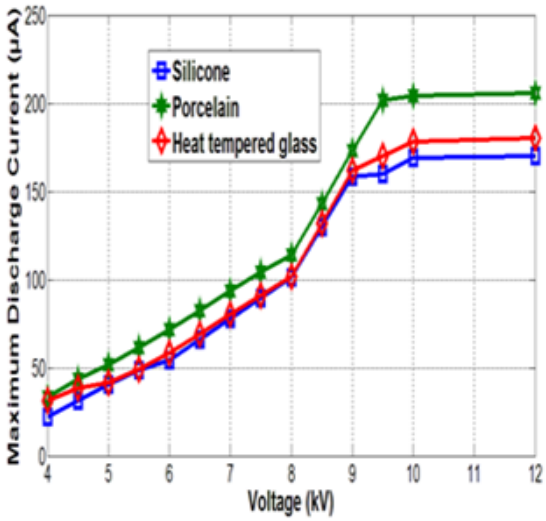


(d) $d = 2.4\,\text{cm}$

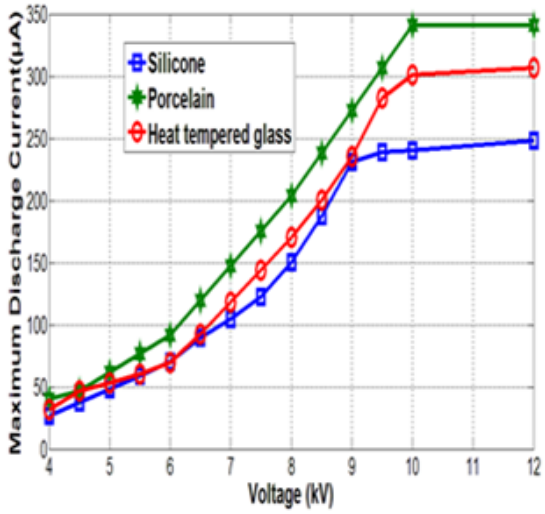


(e) $d = 1.9\,\text{cm}$

***Fig. 5:*** *Variation of $I_0$ against $V$ for the three materials, HV end in Z200 steel, with $D_p = 6\,mm$ and $r = 0.15\,mm$.*

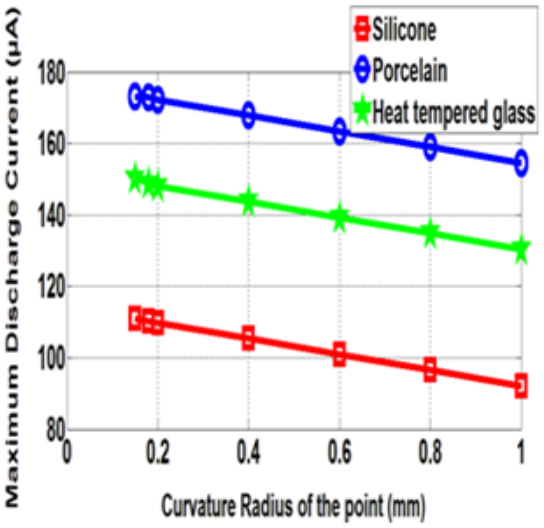


***Fig. 6:*** *Variation of $I_0$ against $r$ for the three materials with $d = 2.9\,cm$, HV end in Z200 steel, with $D_p = 6\,mm$ and $V = 12\,kV$.*

which are shown in Fig. 6. Fig. 6 shows that $I_0$ at the TJ decreases as $r$ increases, thereby improving the dielectric behavior of the three materials.

Indeed, compared to the rest of the insulating surface, load $q$ at the TJ (partially convex surface) moves away from other loads, making it is less affected. The peak effect results in a low repulsive force of accumulated charges at the TJ. The more pointed the HT end, the smaller the tip curvature radius and the greater the charge build-up at this stage, and therefore, the greater the electric field generated by such charges [34].

We consider two HV ends: a large electrode with a large radius $R$ and a small electrode with a small radius $r = R/2$ brought to the same electric potential $V$. Each electrode contains a charge given by the following Eqs. (8) and (9) [35]:

$$q_R = V \times 4\pi\varepsilon_0 R \tag{8}$$

$$q_r = V \times 4\pi\varepsilon_0 r = \frac{V \times 4\pi\varepsilon_0 R}{2} = \frac{q_R}{2} \tag{9}$$

The large pointed electrode will therefore charge twice as much as the small electrode. The electric field $E$ can be calculated as follows [35]:

$$E_R = \frac{V \times R}{d^2} \tag{10}$$

$$E_r = \frac{V \times r}{d^2} = \frac{V \times R/2}{d^2} = \frac{1}{2}\frac{V \times R}{d^2} = \frac{E_R}{2} \tag{11}$$

The field of the large electrode will therefore be twice as important and the same applies to $d$. By becoming closer to their neighborhood, that is to say, the distance from their center, $d = r$ can be written for the small electrode and $d = R$ for the large. This allows us to write Eqs. (12) and (13) as follows:

$$E_R = \frac{V \times R}{R^2} \tag{12}$$

$$E_r = \frac{V \times r}{r^2} = \frac{V \times R/2}{(R/2)^2} = \frac{V \times R/2}{(R^2/4)} = 2\frac{V \times R}{R^2} = 2E_R \tag{13}$$

We then get an electric field at the small electrode twice as large as that of the large electrode. By generalization, if we have a curvature radius $n$ times smaller, the electric field near this electrode is $n$ times greater.

Ultimately, we can say that the electric field increases as an inverse radius function, while the charges $q$ contained in the TJ affected by the electrical potential $V$ increase linearly with the radius. The influence of the curvature radius on the measured current value is in agreement with the work of Hartmann [36].

#### 3.1.4 Influence of the solid insulator permittivity on the maximum discharge current

Figs. 4, 5, and 6 show that whatever the variable studied ($d$, $V$, and $r$), the $I_0$ for three solid insulators (silicone, porcelain, and heat tempered glass) of the same size, with respective relative permittivity ($\varepsilon_r$) (4.2, 6, and 5) is more important for the insulator with the highest $\varepsilon_r$. Indeed, the field in the air at the surface of the solid will be higher as the $\varepsilon_r$ of the latter is high and therefore the value of $I_0$ will also be high [15, 19].

This result is qualitatively in agreement with Toepler's second law (Eq. (14)):

$$\varepsilon_0\varepsilon_r\frac{V_s^2}{e} = \text{Constant} \tag{14}$$

where $e$ is the thickness of the solid insulator and $\varepsilon_0$ is the permittivity of the vacuum.

According to this law, the onset voltage of the sliding discharges ($V_s$) is inversely proportional to the square root of $\varepsilon_r$ in the insulating solid [13]. The relations established by Dakin *et al.* [37] and Halleck [38] indicate the same result.

### 3.2 Results of the Mathematical Models

#### 3.2.1 Monovariable model

The variation of $I_0$ against $d$ obtained experimentally and with the monovariable mathematical model (Eq. (6)) for the three materials are presented in Fig. 7, where $d$ varies between 1.9 and 3.9 cm, $V = 12$ kV, and $r = 0.15$ mm.

The variation of $I_0$ against $V$ obtained experimentally and with the monovariable mathematical model

***Table 1:*** *Statistics for the determination coefficients and errors of the estimating monovariable model.*

| Parameter | Value | | | | | | | | | | | | | | | | | |
|---|---|---|---|---|---|---|---|---|---|---|---|---|---|---|---|---|---|---|
| | $x = d$ | | | $x = V$ | | | | | | | | | | | | | | |
| | | | | $d = 3.9$ cm | | | $d = 3.4$ cm | | | $d = 2.9$ cm | | | $d = 2.4$ cm | | | $d = 1.9$ cm | | |
| | SI | G | P | SI | G | P | SI | G | P | SI | G | P | SI | G | P | SI | G | P |
| RMSE ($\mu$A) | 0.93610 | 0.93008 | 1.2938 | 0.066914 | 0.31601 | 0.14691 | 0.75863 | 0.57706 | 1.5672 | 0.45034 | 0.3115 | 0.70368 | 3.4410 | 2.9273 | 1.6712 | 3.3459 | 3.0386 | 1.5715 |
| MAPE (%) | 0.5067 | 0.3109 | 0.5778 | 0.0443 | 0.1347 | 0.0459 | 1.2875 | 1.1277 | 0.9742 | 0.3758 | 0.2394 | 0.5518 | 2.0840 | 1.4828 | 1.5460 | 1.6368 | 2.3229 | 1.1615 |
| $R^2_{adj}$ | 0.9997 | 0.9998 | 0.9997 | 0.9999 | 0.9983 | 0.9996 | 0.9994 | 0.9998 | 0.9987 | 0.9998 | 0.9999 | 0.9998 | 0.9959 | 0.9972 | 0.9993 | 0.9984 | 0.9991 | 0.9998 |

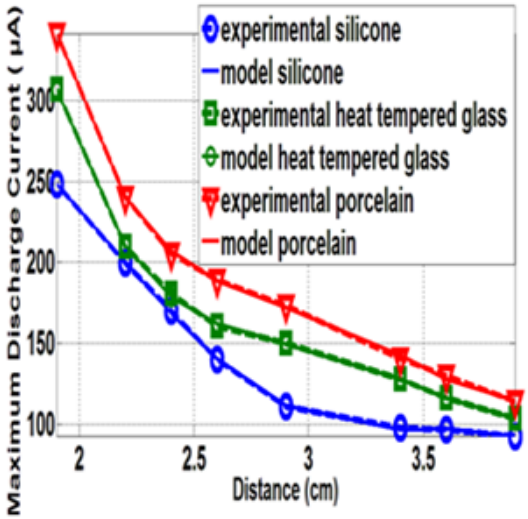


***Fig. 7:*** *Variation of $I_0$ against $d$ obtained experimentally and with the monovariable mathematical model for the three materials where $r = 0.15\,mm$ and $V = 12\,kV$.*

(Eq. (6)) for the three materials are presented in Fig. 8, where $d$ varies between 1.9 and 3.9 cm, $V$ between 4 and 12 kV, and $r = 0.15$ mm.

The variation of $I_0$ against $r$ obtained experimentally and with the monovariable mathematical model (Eq. (6)) for the three materials are presented in Fig. 9, where $r$ varies between 0.15 and 1 mm, $V = 12$ kV and $d = 2.9$ cm.

### 3.2.2 Two-variable quadratic model $V$ and $d$ for the maximum discharge current

The variation of $I_0$ against $d$ and $V$ obtained experimentally and with the two-variable quadratic model (Eq. (7)) for the three materials are presented in Fig. 10, where $V$ varies between 4 and 12 kV, $d$ between 1.9 and 3.9 cm, and $r = 0.15$ mm.

A perfect match can be observed between the experimental results and those of the monovariable and two-variable quadratic mathematical model, with a very small gap (Figs. 7, 8, 9, and 10).

***Table 2:*** *Statistics for the determination coefficients and errors of the estimating two-variable quadradic model.*

| Parameter | Value | | |
|---|---|---|---|
| | SI | G | P |
| RMSE ($\mu$A) | 5.7227 | 5.3764 | 6.0101 |
| MAPE (%) | 9.7516 | 12.1945 | 5.8287 |
| $R^2_{adj}$ | 0.9967 | 0.9980 | 0.9978 |

### 3.2.3 Comparison between the monovariable and two-variable case

We compute the root mean square error (RMSE), mean absolute percentage error (MAPE), and adjusted coefficient of determination ($R^2_{adj}$) for the two types of model. $R^2_{adj}$ measures the adequation of one model, yielded by a regression and the data used to build it [39]. Tables 1 and 2 present the statistics on the errors of the estimating models as well as the determination coefficients (SI, G, and P represent silicone, heat tempered glass, and porcelain, respectively).

As can be observed from Tables 1 and 2, the RMSE and MAPE (%) are small for both models, with the monovariable being even smaller. In the monovariable case (where $x = d$ and $x = V$), the top values are RMSE = 3.4441 $\mu$A and MAPE = 2.3229%. As for the two-variable model, the RMSE varies between 5.3764 and 6.0101 $\mu$A, while MAPE varies between 5.8287 and 12.1945%. Besides, $R^2_{adj}$ shows almost the same value for both models, namely near 0.99.

The RMSE, MAPE, and $R^2_{adj}$ provide information on the precision and performance of the models [40]. Therefore, the results obtained show that the two models under study are precise and exhibit high performance. Moreover, the two-variable quadratic model can evaluate simultaneously and successfully influence $V$ and $d$ on the electric discharge. This leads us to apply the latter on $V$ and $d$ ranges of 10 to 50 kV and 1.9 to 8 cm, respectively.

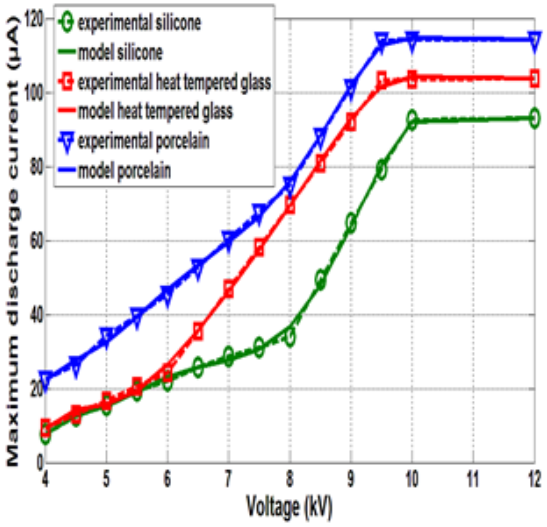


(a) $d = 3.9\,\text{cm}$

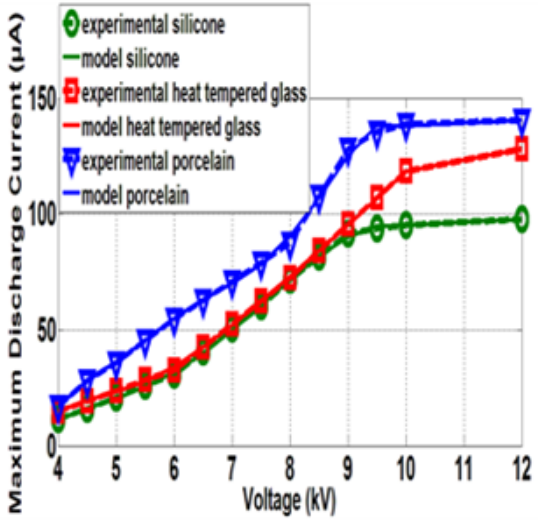


(b) $d = 3.4\,\text{cm}$

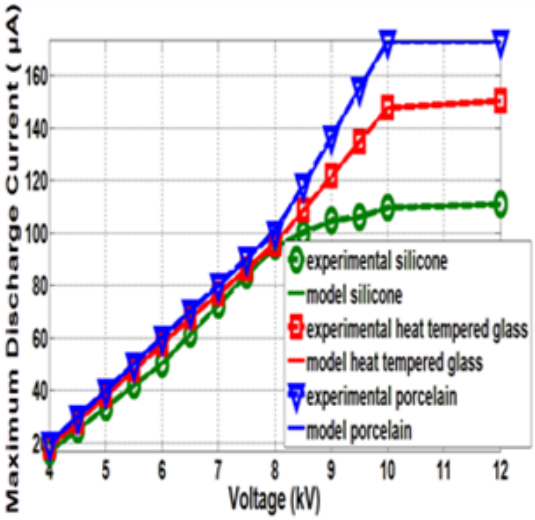


(c) $d = 2.9\,\text{cm}$

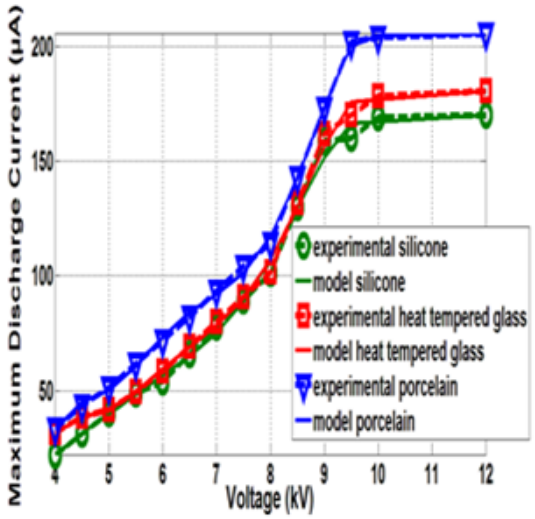


(d) $d = 2.4\,\text{cm}$

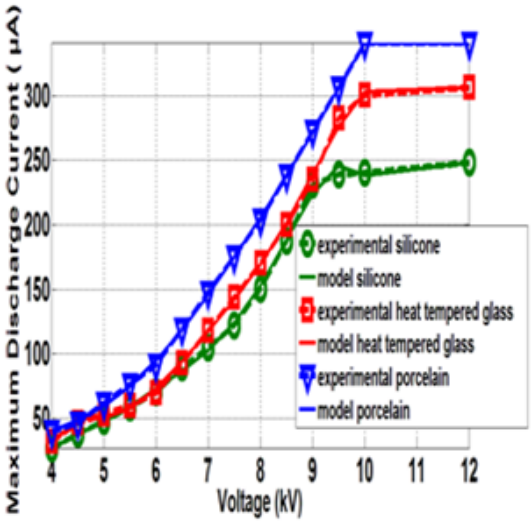


(e) $d = 1.9\,\text{cm}$

***Fig. 8:*** *Variation of $I_0$ against $V$ obtained experimentally and with the monovariable mathematical model for the three materials where $r = 0.15\,mm$.*

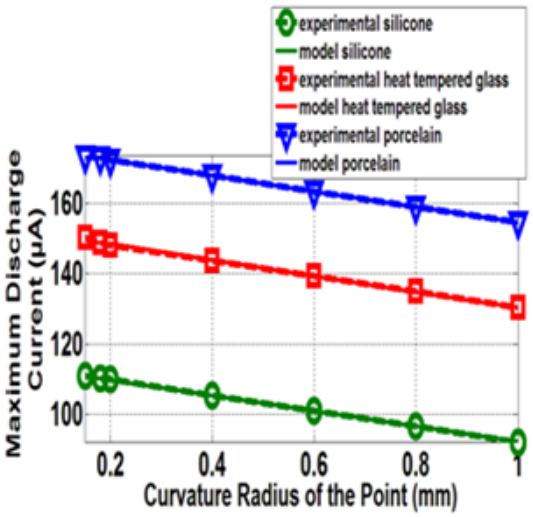


***Fig. 9:*** *Variation of $I_0$ against $r$ obtained experimentally and with the monovariable mathematical model for the three materials where $d = 2.9\,cm$ and $V = 12\,kV$.*

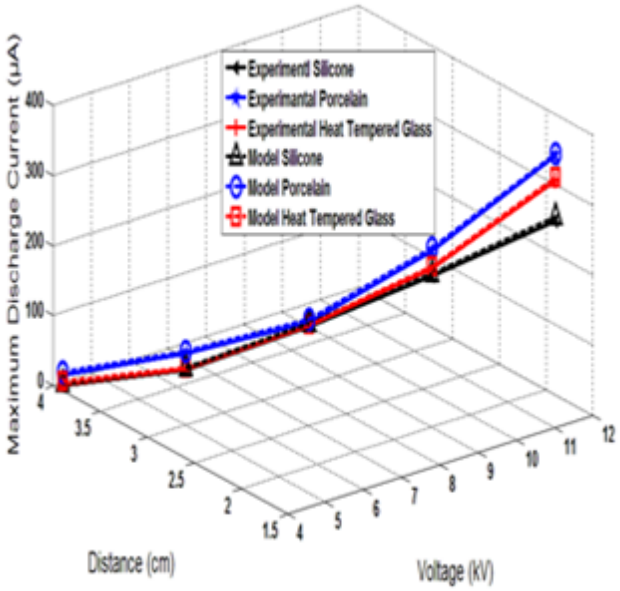


***Fig. 10:*** *Variation of $I_0$ against $d$ and $V$ (4 to 12 kV) obtained experimentally and with the two-variable quadratic mathematical model where $r = 0.15\,mm$ for the three materials.*

#### 3.2.4 Application of the two-variable quadratic model for $V$ and $d$ ranges of 10 to 50 kV and 1.9 to 8 cm, respectively

The model obtained can only be used within the domain of study. Any extrapolation is very risky because it could bring very different results from those expected. A mandatory step before using the model in production would be to test by conducting an experiment at the center of the domain in which our model is to be applied to see whether the value predicted by this model is close to the experimental value. In the case of favorability, it is therefore considered useful to adapt the expression of the model.

**A. Test involving the two-variable quadratic model at the center of the $V$ and $d$ ranges of 10 to 50 kV and 1.9 to 8 cm, respectively**

The variation of $I_0$ against $d$ and $V$ is examined at the center of $V$ and $d$ ranges of 10 to 50 kV and 1.9 to 8 cm, respectively for a variable $V$ between 18 and 34 kV, $d$ between 2 and 4 cm where $r = 0.15$ mm. The results obtained experimentally and with the two-variable quadratic mathematical model (Eq. (7)) for the three materials are presented in Fig. 11.

The modeling results are in full agreement with the experimental data, exhibiting a very small error range. This enables us to employ this model in the $V$ and $d$ ranges of 10 to 50 kV and 1.9 to 8 cm, respectively.

In addition, the validation of the two-variable quadratic model demonstrates its precision and feasibility.

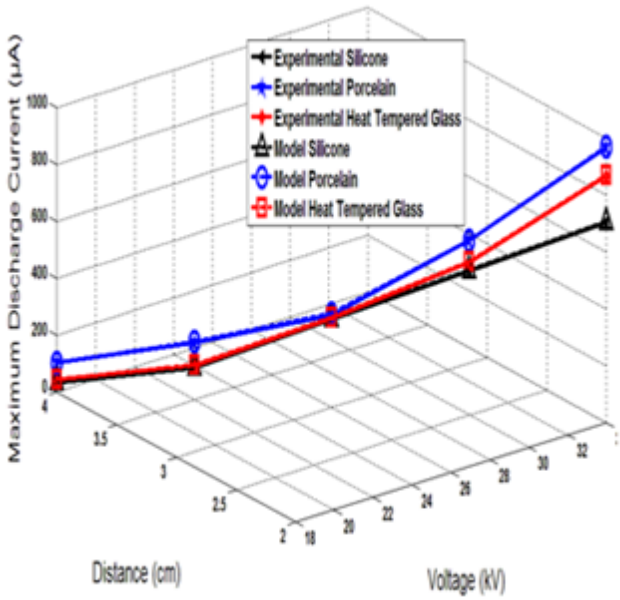


***Fig. 11:*** *Variation of $I_0$ against $d$ and $V$ (18 to 34 kV) obtained experimentally and with the two-variable quadratic mathematical model where $r = 0.15\,mm$ for the three materials.*

**B. Two-variable quadratic model on $V$ and $d$ ranges of 10 to 50 kV and 1.9 to 8 cm, respectively**

The variation of $I_0$ against $d$ and $V$ obtained from the two-variable quadratic mathematical model (Eq. (7)) for the three materials is presented in Table 3, where $d$ varies between 1.9 and 8 cm and

***Table 3:*** *Variation of $I_0$ against $d$ and $V$, for $V$ and $d$ ranges of 10 to 50 kV and 1.9 to 8 cm, respectively, for the three materials obtained from the two-variable quadratic mathematical model.*

| Parameter | Value | | | | | | | | | | |
|---|---|---|---|---|---|---|---|---|---|---|---|
| $V$ (kV) | 10 | 15 | 20 | 30 | 38 | 40 | 42 | 44 | 46 | 48 | 50 |
| $d$ (cm) | 1.9 | 2 | 3 | 4 | 4.5 | 5 | 5.5 | 6 | 6.5 | 7 | 8 |
| $I_0$ of the silicone: $I_{0SI}$ ($\mu$A) | 211.08 | 235.34 | 305.1 | 467.32 | 520.76 | 610.55 | 689.62 | 721.18 | 770.56 | 805.09 | 868.45 |
| $I_0$ of the porcelain: $I_{0P}$ ($\mu$A) | 286.67 | 310.27 | 322.03 | 543.55 | 595.45 | 681.88 | 766.21 | 795.35 | 841.57 | 876.69 | 948.58 |
| $I_0$ of the heat tempered glass: $I_{0G}$ ($\mu$A) | 258.78 | 286.42 | 310.70 | 515.19 | 569.73 | 657.34 | 730.20 | 766.81 | 813.96 | 848.58 | 914.12 |

$V$ between 10 and 50 kV, with $r$ set to 0.15 mm.

Table 3 indicates that for $r = 0.15$ mm and the three materials under study (silicone, porcelain, and heat tempered glass) in $V$ and $d$ ranges of 10 to 50 kV and 1.9 to 8 cm, respectively, the silicone insulators have the smallest discharge current (the electric discharges are small), whatever the $V$ and its corresponding $d$.

## 4. CONCLUSION

In this paper, the discharge current was studied experimentally for three types of insulating materials, namely silicone, porcelain, and heat tempered glass. The discharge current is strongly influenced by the permittivity of the solid insulator, which is higher for the insulators with high permittivity (porcelain and heat tempered glass). However, the surface discharges are even shorter and less ramified when the dielectric permittivity is lower (the silicone insulator presents better performance than porcelain and heat tempered glass). In addition, the pre-breakdown currents are higher when the applied voltage is higher and the inter-electrode distance is smaller. Besides, the discharges are highly dependent, increasing with the decrease in the curvature radius of the tip.

The benefit of modeling the current by a polynomial lies in the researcher's ability to calculate all the responses of the domain of study without being complied to perform experiments. However, the proposed regression models of the electric discharge current (monovariable and two-variable quadratic) provide a precise and reasonable estimate of the optimal currents against the three variables applied, namely voltage, inter-electrode distance, and curvature radius. The two models offer two major advantages. Firstly, they have great representation capacity, and can successfully yield the different relations of the variables with respect to the maximum electric discharge $I_0$, with no change in structure required. Secondly, the related optimization problem is easy to solve, subsequently optimizing the precision and computing speed.

Moreover, the two-variable quadratic model can provide information about the influence of the two variables, voltage and distance, on the electric discharge at the same time. The determination coefficient $R^2_{adj}$ is around 0.99, revealing that 99% of the maximum discharge current variation can be justified by a change in two variables. This is why we validated the two-variable quadratic model and applied it to the voltage and distance ranges of 10 to 50 kV and 1.9 to 8 cm, respectively.

Finally, this study provides us with new applicable knowledge concerning the triple-junction effect on electrical insulation with recommendations for optimizing its design for superior performance.

In perspective, we recommend:

1. An increase in the current leakage path of the electric insulator.
2. An increase in the curvature radius of the triple junction on an electric insulator.
3. The selection of an appropriate type of insulator. Indeed, silicone has the highest dielectric performance for application in the industrial field.
4. Simulation of the results found by COMSOL software.
5. Experimental characterization of the same gas (air), metal, and solid insulators under direct current.
6. Experimental characterization of other types of material in the presence of different gases and mixtures (ecological) under alternating, direct and impulsive currents.
7. Quantitative charge distribution on the insulator starting from the triple junction through the application of numerical approaches such as the "inverse method".

## REFERENCES

[1] T. Nitta, Y. Shibuya, Y. Fujiwara, Y. Arahata, H. Takahashi, and H. Kuwahara, "Factors controlling surface flashoverin SF6 gas insulated systems," *IEEE Transactions on Power Apparatus and Systems*, vol. 97, no. 3, pp. 959–968, 1978.

[2] A. S. Pillai, R. Hackam, and P. H. Alexander, "Influence of radius of curvature contact angle and material of solid insulator on the electric field in vacuum (and gaseous) gaps," *IEEE Transactions on Electrical Insulation*, vol. 18, no. 1, pp. 11–22, 1983.

[3] Y. Hattab and N. Benharrats, "Study of the electrical and thermal degradation of polyaniline in an aggressive environment," (in French),

*The Canadian Journal of Chemical Engineering*, vol. 94, no. 12, pp. 2303–2314, 2016

[4] A. H. Cookson, "Gas-insulated cables," *IEEE Transactions on Electrical Insulation*, vol. 20, no. 5, pp. 859–890, 1985.

[5] T. S. Sudarshan and R. A. Dougal, "Mechanisms of surface flashover along solid dielectrics in compressed gases: a review," *IEEE Transactions on Electrical Insulation*, vol. 21, no. 5, pp. 727–746, 1986.

[6] T. W. Dakin and J. Lim, "Corona Measurement and Interpretation," *Transactions of the American Institute of Electrical Engineers. Part III: Power Apparatus and Systems*, vol. 76, no. 3, pp. 1059–1065, 1957.

[7] G.-Q. Su *et al.*, "Influence of Flashover Initiation Process on Surface Insulation Performance for Insulators under Impulse Voltage in Vacuum," in *2019 IEEE Conference on Electrical Insulation and Dielectric Phenomena (CEIDP)*, Richland, WA, USA, 2019, pp. 230–233.

[8] P. A. Chatterton and D. K. Davies, "Secondary electron emission characteristics of insulator surfaces before and after impulse flashover," in *Proceedings of the VIIIth International Symposium on Discharges and Electrical Insulation in Vacuum*, Albuquerque, NM, USA, 1978, pp. d2-1–d2-11.

[9] L. Cai, J. Wang, X. Zhu, X. Wang, Y. Wang, and D. Zhang, "Two-dimensional simulation research of secondary electron emission avalanche discharge on vacuum insulator surface," *Physics of Plasmas*, vol. 22, no. 1, pp. 1–8, 2015.

[10] Y. S. Naidu and G. V. N. Kumar, "Minimisation of electric field stress at triple junction of a functionally graded cone type spacer in a gas insulated busduct with metal inserts," *High Voltage*, vol. 2, no. 2, pp. 110–118, 2017.

[11] D. D. Chowdary and J. Amarnath, "Electric field analysis at the triple junction of a optimum profile disc type spacer in SF6 gas insulated system with abnormalities under DC voltages," in *2011 Annual Report Conference on Electrical Insulation and Dielectric Phenomena*, Cancun, Mexico, 2011, pp. 215–218.

[12] M. S. Chung, A. Mayer, N. M. Miskovsky, B. L. Weiss, and P. H. Cutler, "Dielectric effect on electric fields in the vicinity of the metal-vacuum-dielectric junction," *Ultramicroscopy*, vol. 132, pp. 41–47, 2013.

[13] L. Yang, H. Xu-Dong, F. Yu-Jun, and H. Hong-Liang, "Controlling Factors of the Electric Field at the Triple Junction," *Chinese Physics Letters*, vol. 31, no. 2, 2014, Art. no. 027701.

[14] A. Beroual and L. Kebbabi, "Influence of the voltage waveform and hydrostatic pressure on morphology and final length of discharges propagating over solid-liquid interfaces," *IEEE Transactions on Dielectrics and Electrical Insulation*, vol. 16, no. 6, pp. 1574–1581, 2009.

[15] M. A. Handala and O. Lamrous, "Study of pre-breakdown current in air-solid interface," in *2009 IEEE 9th International Conference on the Properties and Applications of Dielectric Materials*, Harbin, China, 2009, pp. 713–716.

[16] A. Abahazem, N. Merbahi, H. Guedah, and M. Yousfi, "Electric and Spectroscopic Studies of Pulsed Corona Discharges in Nitrogen at Atmospheric Pressure," *Journal of Analytical Sciences, Methods and Instrumentation*, vol. 7, no. 3, pp. 57–74, 2017.

[17] J. Zhang, Y. F. Guo, D. Z. Pan, and K. M. Yang, "A Novel 3-D Analytical Method for Curvature Effect-Induced Electric Field Crowding in SOI Lateral Power Device," *IEEE Transactions on Electron Devices*, vol. 63, no. 11, pp. 4359-4365, 2016.

[18] S. Okabe, "Phenomena and mechanism of electric charges on spacers in gas insulated switchears," *IEEE Transactions on Dielectrics and Electrical Insulation*, vol. 14, no. 1, pp. 46–52, 2007.

[19] T. Tokunaga, S. Nishikawa, T. Sakoda, and T. Fukano, "Influence of triple-junction on sparkover voltage for a series gap of arrester," in *2013 IEEE Electrical Insulation Conference (EIC)*, Ottawa, ON, Canada, 2013, pp. 110–113.

[20] A. Jain and A. K. Pandey, "Multiple Quality Optimizations in Electrical Discharge Drilling of Mild Steel Sheet," *Materials Today: Proceedings*, vol. 4, no. 8, pp. 7252–7261, 2017.

[21] S. P. Arikatla, K. T. Mannan, and A. Krishnaiah, "Parametric Optimization in Wire Electrical Discharge Machining of Titanium Alloy Using Response Surface Methodology," *Materials Today: Proceedings*, vol. 4, no. 2, pp. 1434–1441, 2017.

[22] A. Hafeez *et al.*, "Optimization on cleaner intensification of ozone production using Artificial Neural Network and Response Surface Methodology: Parametric and comparative study," *Journal of Cleaner Production*, vol. 252, 2020, Art. no. 119833.

[23] M. H. Dehghani, K. Yetilmezsoy, M. Salari, Z. Heidarinejad, M. Yousefi, and M. Sillanpaa, "Adsorptive removal of cobalt (II) from aqueous solutions using multi-walled carbon nanotubes and $\gamma$-alumina as novel adsorbents: Modelling and optimization based on response surface methodology and artificial neural network," *Journal of Molecular Liquids*, vol. 299, 2020, Art. no. 112154.

[24] D. D. Gawali, A. Zidna, and P. S. V. Nataraj, "lgorithms for unconstrained global optimization of nonlinear (polynomial) programming problems: the single and multi-segment polynomial

B-spline approach," *Computers and Operations Research*, vol. 87, pp. 205–220, 2017.

[25] M. Gangil and M. K. Pradhan, "Modeling and optimization of electrical discharge machining process using RSM: A review," *Materials Today: Proceedings*, vol. 4, no. 2, Part A, pp. 1752–1761, 2017.

[26] A. Larsson, P. Lalande, A. Bondiou-Clergerie, P. Lalande, and A. Delannoy, "The lightning swept stroke along an aircraft in flight, Part I: thermodynamic and electric properties of lightning arc channels," *Journal of Physics D: Applied Physics*, vol. 33, no. 15, pp. 1866–1875, 2000.

[27] E. R Shaaban, F. Diab, G. M. El-Kashef, K. M. Ahmed, M. E. Abdel-kader, and W. H. Gaber, "Effect of inter-electrode distances of glow discharge on structural and optical properties of ZnSe," *Journal of Nanotechnology & Advanced Materials*, vol. 4, no. 2, pp. 45–51, 2016

[28] V. Gagliardo, "Discharges in very-short air gaps in plane-parallel electrodes and under AC voltage," *IEEE Transactions on Dielectrics and Electrical Insulation*, vol. 1, no. 6, pp. 1156–1166, 1944.

[29] M. E. Slama and A. Beroul, "Behavior of AC High Voltage Polyamide Insulators: Evolution of Leakage Current in Different Surface Conditions," *Power Engineering and Electrical Engineering*, vol. 13, no. 2, pp. 74–80, 2015.

[30] N. Jordan, Y. Y. Lau, D. M. French, R. M. Gilgenbach, and P. Pengvanich, "Electric field and electron orbits near a triple point," *Journal of Applied Physics*, vol. 102, no. 3, pp. 1–10, 2007.

[31] H. Javadiz, M. Farzaneh, H. Hemmatjou, and I. Fofana, "An analytic model to simulate leakage current of a snow-covered insulator," *European Transactions on Electrical Power*, vol. 18, no. 4, pp. 403–422, 2008.

[32] K. V. Kozlov, R. Brandenburg, H. E. Wagner, A. M. Morozov, and P. Miche, "Investigation of the filamentary and diffuse mode of barrier discharges in $N_2/O_2$ mixtures at atmospheric pressure by cross-correlation spectroscopy," *Journal of Physics D: Applied Physics*, vol. 38, no. 4, pp. 518–529, 2005.

[33] O. Eichwald, O. Ducasse, D. Dubois, A. Abahazem, N. Merbahi, M. Benhenni, and M. Yousfi, "Experimental analysis and modelling of positive streamer in air: towards an estimation of O and N radical production," *Journal of Physics D: Applied Physics*, vol. 41, no. 23, pp. 1–11, 2008.

[34] M. Rezinkina, O. Rezinkin, F. D'Alessandro, A. Danyliuk, A. Guchenko, and S. Lytvynenko, "Experimental and modeling study of the dependence of corona discharge on electrode geometry and ambient electric field," *Journal of Electrostatics*, vol. 87, pp. 79–85, 2017.

[35] E. Durand, *Électrostatique*, vol. II, Paris, France: Masson et Cie, 1966.

[36] G. Hartmann, "Theoretical evaluation of Peek's law," *IEEE Transactions on Industry Applications*, vol. 20, no. 2, pp. 1647–1651, 1984.

[37] T. W. Dakin, H. M. Philofsky, and W. C. Divens, "Effect of electric discharges on the breakdown of solid insulation," *Transaction of the American Institute of Electrical Engineers, Part I: Communication and Electronics*, vol. 73, no. 2, pp. 155–162, 1954.

[38] M. C. Halleck, "Calculation of corona starting voltage in air-solid dielectric systems," *Transactions of the American Institute of Electrical Engineers, Part III: Power Apparatus and Systems*, vol. 75, no. 3, pp. 211–216, 1956.

[39] S. Kiliç, "Linear regression analysis," (in Turkish), *Journal of Mood Disorders*, vol. 13, no. 2, pp. 90–92, 2013.

[40] A. Capozzoli, D. Grassi, and F. Causone, "Estimation models of heating energy consumption in schools for local authorities planning," *Energy Build*, vol. 105, no. 15, pp. 302–313, 2015.

**Nabila Saim** received her M.Sc.Eng. degree in Electrical Engineering from Mouloud Mammeri University of Tizi-Ouzou, Algeria, in 2010 and the M.Sc. degree in Electrical Engineering at the same University in 2011. She is currently a Ph.D. student and a part-time lecturer at the Mouloud Mammeri University of Tizi-Ouzou. Her main interests include high voltage engineering, dielectric materials, surface discharges and electrical insulation.

**Ferroudja Bitam-Megherbi** receive her Magister degree in 1996. Her doctorate thesis which was devoted to dielectric materials has been achieved in 2007. She presently is a Professor at the Electrical Engineering Department in Mouloud Mammeri University of Tizi-Ouzou. Her domain of interest concerns electrical insulation and the magnetic materials. The results of her works appear in different publications relating to dielectric and magnetic materials behaviour.